

# Catalysis Science & Technology

Accepted Manuscript



This is an *Accepted Manuscript*, which has been through the Royal Society of Chemistry peer review process and has been accepted for publication.

*Accepted Manuscripts* are published online shortly after acceptance, before technical editing, formatting and proof reading. Using this free service, authors can make their results available to the community, in citable form, before we publish the edited article. We will replace this *Accepted Manuscript* with the edited and formatted *Advance Article* as soon as it is available.

You can find more information about *Accepted Manuscripts* in the [Information for Authors](#).

Please note that technical editing may introduce minor changes to the text and/or graphics, which may alter content. The journal's standard [Terms & Conditions](#) and the [Ethical guidelines](#) still apply. In no event shall the Royal Society of Chemistry be held responsible for any errors or omissions in this *Accepted Manuscript* or any consequences arising from the use of any information it contains.



Journal Name

ARTICLE

## Fe-Mn-Cu/SiO<sub>2</sub>@Silicalite-1 Catalyst for CO Hydrogenation: Role of Zeolite Shell on Light-Olefin Production

Weilin Song,<sup>a,b</sup> Bin Zhang,<sup>a</sup> Lifeng Chen,<sup>a</sup> Jing Shi,<sup>b</sup> Xiaowei Cheng,<sup>a</sup> Lianghua Wu,<sup>b</sup> Weimin Yang,<sup>b</sup> Jian Zhou,<sup>b</sup> Yahong Zhang,<sup>a</sup> Yuewu Tao,<sup>b</sup> Yi Tang<sup>\*,a</sup>

Received 00th January 20xx,  
Accepted 00th January 20xx

DOI: 10.1039/x0xx00000x

www.rsc.org/

Core-shell structured catalyst is considered effective for regulating product distribution in complex reaction network. By systematically analyzing the behaviors of Fe-Mn-Cu/SiO<sub>2</sub>@silicalite-1 core-shell catalyst in Fischer-Tropsch synthesis, a unique temperature-dependent role of silicalite-1 shell is demonstrated on the distribution of products via modulation of the intra- and inter-pellet secondary reactions, which successfully fulfills synchronous increments of CO conversion, light olefin/light paraffin ratio ( $C_{2-4}^{\omega}/C_{2-4}^{\text{p}}$ ) and  $C_{2-4}^{\omega}$  selectivity, opposite to the behavior of naked industrial Fe-Mn-Cu/SiO<sub>2</sub> catalyst. This effect could be attributed to the different diffusion limitation of silicalite-1 shell on various reactants/products in different temperature ranges. Such a discovery not only rationally explains the excellent performance of the core-shell catalyst on  $C_{2-4}^{\omega}$  production but also provides a new clue for the design of catalysts in complex reaction networks.

### 1. Introduction

Light olefins ( $C_{2-4}^{\omega}$ ), which are traditionally obtained from petroleum resources, are very important raw materials for chemical industry. Due to the limited resources of crude oil, it is necessary to develop  $C_{2-4}^{\omega}$  production via non-petroleum routes for the future chemical industry. In recent years, there has been growing interest in producing  $C_{2-4}^{\omega}$  by syngas that is derived from coal, natural gas and renewable biomasses. So far, the two-step processes have been well established to provide  $C_{2-4}^{\omega}$  from intermediates of methanol or hydrocarbons, which can be obtained from syngas.<sup>1-5</sup> Obviously, it is more promising to produce  $C_{2-4}^{\omega}$  via direct transformation of syngas.<sup>6-8</sup> Fischer-Tropsch synthesis (FTS) has been reported to convert syngas into flexible products, including olefins, liquid hydrocarbons, waxes and oxygenates. Among these products, the linear  $\alpha$ -olefins are the most important, which could be further applied to synthesize high valued polymers and other chemicals.<sup>9</sup> However, they usually suffer from low selectivity because of their proneness to be hydrogenated<sup>10</sup> and/or initiate the chain-growth reactions.<sup>11, 12</sup> Particularly, it is difficult to selectively produce  $C_{2-4}^{\omega}$  due to intensive secondary reactions.<sup>13-15</sup>

Various reaction mechanisms of FTS have been proposed in the past decades, which generally include the following steps: (1) CO and H<sub>2</sub> molecules diffuse into the pores of FTS catalyst pellets and are adsorbed on their surface; (2) The primary

products (such as  $\alpha$ -olefins) are generated via CO hydrogenation, which can be further transformed into paraffins via hydrogenation and/or long-chain hydrocarbons via chain-growth reactions during transferring from the interior pores of catalyst pellets to gaseous phase (denoted as intra-pellet secondary reactions); And (3) the obtained  $\alpha$ -olefin products may further re-diffuse into other pellets in the downstream of catalyst bed, and would lead to the secondary reactions once again to form paraffins and/or long chain hydrocarbons (denoted as inter-pellet secondary reactions). Obviously, both of the intra- and inter-pellet secondary reactions will reduce selectivity of  $\alpha$ -olefin products, especially the active light olefins.<sup>16-19</sup>

It has been reported that the intra-pellet secondary reactions are closely related to the density of active sites (reaction rate) and diffusion limitation of pores of catalysts.<sup>13, 20, 21</sup> The latter is determined by the catalyst pellet size (diffusion distance) and the pore radius (diffusion resistance). Diffusion limitation on reactants results in a higher intra-pellet H<sub>2</sub>/CO ratio than that in gaseous reactant flow because of the relatively slower diffusion rate of CO.<sup>16, 17</sup> The high intra-pellet H<sub>2</sub>/CO ratio will naturally lead to paraffinic products due to enhanced secondary hydrogenation of  $\alpha$ -olefins.<sup>22-27</sup> Besides, slow mass transfer of products causes long intra-pellet residence time, and thus brings on serious intra-pellet secondary reactions. This issue has been verified by the phenomena of lower olefin contents in catalysts with a larger pellet size.<sup>17, 20</sup> It is also proved by lower olefin/paraffin ratio in longer chain hydrocarbon products due to their low diffusion rate.<sup>15, 28</sup> Although light  $\alpha$ -olefins possess a higher diffusion rate than their long chain analogs, their higher activity for secondary reactions results in lower olefin/paraffin ratio in final

<sup>a</sup> Department of Chemistry, Shanghai Key Laboratory of Molecular Catalysis and Innovative Materials, Laboratory of Advanced Materials and Collaborative Innovation Center of Chemistry for Energy Materials, Fudan University, 220 Handan Road, Shanghai 200433, China.

<sup>b</sup> Shanghai Research Institute of Petrochemical Technology, SINOPEC, 1658 Pudong North Road, Shanghai 201208, China.

products.<sup>20, 29, 30</sup> In our previous work,<sup>31</sup> a novel silica nanowire-supported iron catalyst with open structure was proved to greatly reduce intra-pellet secondary reactions and thereby improve the olefin/paraffin ratio in C<sub>2</sub>-C<sub>4</sub> products (denoted as C<sub>2-4</sub><sup>=</sup>/C<sub>2-4</sub><sup>0</sup>) and C<sub>2-4</sub><sup>=</sup> selectivity.

The inter-pellet secondary reaction is another factor influencing selectivity, which seriously depends on bed residence time.<sup>16, 19, 32</sup> Some controlled experiments in consecutive and recycle reactors were conducted to prove the effects of inter-pellet secondary reaction.<sup>18, 22</sup> The former shows that light olefins produced in the first reactor can take part in secondary reactions in the second reactor, while the latter illustrates that olefin products can convert into secondary products when they are recycled back into the reactor. Furthermore, inter-pellet secondary reactions have also been proved by co-feeding experiments. The added light  $\alpha$ -olefin inlets are prone to participate in secondary reactions because of their high activity and the activity order is ethylene > propylene > 1-butylene.<sup>33-38</sup>

Major efforts have been made to reduce the secondary reactions of  $\alpha$ -olefins. Monolithic reactors are generally considered to reduce diffusion limitation and improve olefin selectivity in FTS. It has been presented that diffusion limitation could be avoided if the active coating is thinner than 50  $\mu\text{m}$ .<sup>24, 25</sup> In this case, a higher C<sub>6</sub><sup>+</sup> olefin selectivity is achieved. It has also been found that the supercritical operation can obviously improve  $\alpha$ -olefin selectivity via suppressing secondary reactions.<sup>32, 39, 40</sup> Furthermore,  $\alpha$ -olefin contents also can be increased markedly and are almost independent of chain length in the C<sub>6</sub><sup>+</sup> range if a polar polymer of polyethylene glycol is added. The negligible solubility of  $\alpha$ -olefins in the polar liquid could result in rapid escape of  $\alpha$ -olefins from catalyst pellets, leading to low probability of secondary reactions.<sup>41</sup> These measures can raise the  $\alpha$ -olefins content in products, especially for those of long chain  $\alpha$ -olefins. However, their effects on light olefins are unclear.

Very recently, novel core-shell structured catalysts are proposed to improve light olefin selectivity. A core-shell structured catalyst with Fe/SiO<sub>2</sub> core and silicalite-1 shell has been reported to probably enhance the intra-pellet H<sub>2</sub>/CO ratio which is beneficial for producing light hydrocarbons.<sup>42</sup> Additionally, a catalyst with cobalt nanoparticles enwrapped with a silica shell shows higher C<sub>2-4</sub><sup>=</sup> selectivity than the conventional silica supported cobalt catalyst.<sup>43</sup> They suggest that the inert shells inhibit secondary reactions of C<sub>2-4</sub><sup>=</sup>.<sup>42, 43</sup> However, the relationship between structure and performance remains obscure due to the difficulty to determine their propositions under FTS conditions. In our work, for the first time as we accessed, a unique temperature-dependent effect of a zeolite shell on C<sub>2-4</sub><sup>=</sup> production is revealed. It is implemented through systematically studying the FTS reaction behaviors on a specially designed core-shell structured catalyst of Fe-Mn-Cu/SiO<sub>2</sub>@silicalite-1 (FTC@S1) composed of a silicalite-1 shell and an industrial Fe-Mn-Cu/SiO<sub>2</sub> (FTC) core. Different from the naked FTC catalyst, the core-shell FTC@S1 catalyst successfully fulfills synchronous increase of CO conversion and C<sub>2-4</sub><sup>=</sup> selectivity at high temperature. The

pivotal effects of the silicalite-1 shell on intra-/inter-pellet secondary reactions at low/high temperatures are evidently proposed to illustrate the peculiar temperature-dependent performance of the core-shell catalyst. Such discovery not only can rationally explain the excellent performance in producing C<sub>2-4</sub><sup>=</sup> by the core-shell catalyst but also affords a rational clue for the design of catalysts for complex reaction networks.

## 2. Experimental

### 2.1 Catalyst Preparation

FTC core catalyst is obtained by a typical precipitation and spray dry method. Typically, 600 g of Fe(NO<sub>3</sub>)<sub>3</sub>•9H<sub>2</sub>O is dissolved in 1000 g of water, and 25% (w/w) ammonia is added into the solution until the pH reaches 7.5. The precipitate is filtered and washed with deionized water, followed by adding 500 g of 50% (w/w) Mn(NO<sub>3</sub>)<sub>2</sub> and 15 g of Cu(NO<sub>3</sub>)<sub>2</sub>•3H<sub>2</sub>O. Afterwards, 100 g of 40% (w/w) silica sol is added to form slurry which is then spray dried, and the powder is calcined in a rotary furnace at 873 K for 4 h to obtain the final FTC core catalyst. The average size of FTC is 59.5  $\mu\text{m}$ .

The core-shell structured FTC@S1 catalyst is prepared by a hydrothermal synthesis method. The pre-prepared FTC core catalyst is firstly coated with silicalite-1 seeds (average 87 nm) by a layer-by-layer method via alternative adsorption of diallyldimethylammonium chloride (aqueous solution of 1.5 wt%, solid/solution ratio of 1 g/10 mL) and silicalite-1 seeds (as-prepared suspension of 10 wt%).<sup>44</sup> Afterwards, 10 g of seeded FTC pellets are added into 470 g of synthesis solution (SiO<sub>2</sub>:TPAOH:H<sub>2</sub>O=1:0.4:320) and transferred into a Teflon-lined autoclave. The hydrothermal synthesis procedure is performed at 423 K for 24 h. The final core-shell structured FTC@S1 catalysts is obtained by rinsing the solid with deionized water for several times until the pH=7, and drying the solid at 373 K overnight and then calcining it at 823 K for 6 h to remove the organic structure directing agent (SDA).

### 2.2 Catalyst Characterization

Scanning electron microscopic (SEM) images are obtained on a Philips XL30 instrument with accelerating voltages of 20 kV. X-ray diffraction (XRD) patterns are obtained on a Rigaku D/MAX-RB diffractometer over a 2 $\theta$  range of 5–80° with CuK $\alpha$  radiation. N<sub>2</sub>-sorption isotherms are measured by a Micromeritics ASAP-2010 instrument at liquid nitrogen temperature. X-ray photoelectron spectrum (XPS) is obtained on an AXIS Ultra DLD instrument.

The acid extraction experiment is carried out by dipping 0.5 g of FTC or 0.7 g of uncalcined FTC@S1 (i.e., with SDA in its micropores) in excess amount of HCl solution (30 mL, 1 mol L<sup>-1</sup>), at 353 K for 3 days. Afterwards, the solids are filtered, washed, dried, calcined and grinded. Their Fe and Mn contents are tested by inductively coupled plasma-atomic emission spectrometry (ICP-AES). Additionally Fe and Mn contents in FTC and FTC@S1 before acid-extraction are also determined by ICP-AES. All results are calculated based on the weight of calcined catalysts.

### 2.3 FTS test

FTS experiments are conducted in an 8 mm i. d. stainless steel fixed bed reactor. For the test on FTC catalyst, 1 g of catalyst is loaded in the reactor and reduced with  $\text{H}_2$  ( $50 \text{ ml}\cdot\text{min}^{-1}$ ) at 723 K and 1.0 MPa for 8 hours. For the test on FTC@S1, 1.2 g of catalyst is used to guarantee the same loading amount of active component and pre-treated under the same condition. Then, a syngas flow is introduced into the reactor with  $\text{N}_2$  as internal standard.  $\text{N}_2/\text{syngas}$  (v/v) ratio is 1/8, and  $\text{H}_2/\text{CO}$  ratio (v/v) is 3/2 and the weight hourly space velocity (WHSV) was  $3.9 \text{ g}\cdot\text{h}^{-1}\cdot(\text{g Fe})^{-1}$  except being indicated. Each reaction result under different conditions is obtained from a new run by reloading catalyst. The products are analyzed by two on-line gas chromatographers (Agilent 7890A GC) with a flame ionization detector (FID) and a thermal conductivity detector. Agilent HP-1, HP-AL/M and Hayesep-D columns are used to separate the hydrocarbons, light olefins and other gaseous components, respectively.

### 2.4 Ethylene hydrogenation

To simulate secondary reactions of olefins in FTS, an ethylene hydrogenation reaction is conducted on both catalysts of FTC and FTC@S1. The loading amounts of catalysts are the same as those in the FTS test (Section 2.3). To ensure the similar active component state of catalysts with that in FTS, the catalysts are firstly reduced with  $\text{H}_2$  at 723 K and 1.0 MPa for 8 hours, and then syngas is introduced into the reactor at 623 K and 1.0 MPa for 24 hours with WHSV of  $3.9 \text{ g}\cdot\text{h}^{-1}\cdot(\text{g Fe})^{-1}$  and  $\text{H}_2/\text{CO}$  ratio of 3/2. Afterwards, the reactant gas is switched to a mixing gas flow of  $\text{H}_2$  and ethylene, and the reactor is adjusted to corresponding temperature and pressure for ethylene hydrogenation. The products are analyzed by an on-line Agilent 7890 GC with a FID.

## 3. Results

### 3.1 Catalyst characterization

SEM images of FTC and FTC@S1 catalysts are shown in Figure 1. The pellets of FTC@S1 after hydrothermal treatment (Figure 1-B1) well maintain the initial spherical shape of parent FTC cores (Figure 1-A1). The SEM image at high magnification clearly shows that surface of the core sphere (FTC, Figure 1-A2) is covered by a layer of inter-grown zeolite nano-crystals with sizes of about 200-600 nm (FTC@S1, Figure 1-B2). The image of the cross section of FTC@S1 shows the intact zeolite shell with thickness of about  $2.4 \mu\text{m}$  (Figure 1-B3) around the core catalyst. XRD pattern of the FTC core catalyst possesses only the characteristic peaks of  $\alpha\text{-Fe}_2\text{O}_3$  in the range of  $33\text{-}36^\circ/2\theta$  (Figure 2a), while that of FTC@S1 catalyst exhibits peaks of both  $\alpha\text{-Fe}_2\text{O}_3$  and typical MFI framework in the range of  $7.0\text{-}10.0$  and  $23.0\text{-}25.0^\circ/2\theta$  (Figure 2-A). No impure phase is detected on XRD and elements of Fe, Mn and Cu are absent in XPS testing, indicating that the core catalyst is well retained and enwrapped during the shell formation process. The weight of samples increase about 20% after hydrothermal treatment, implying the crystallization of silicalite-1 on FTC.

Correspondingly, the amounts of Fe and Mn in original FTC are also about 20% more than those in FTC@S1 (Table 1) due to the introduction of silicalite-1 in the latter.

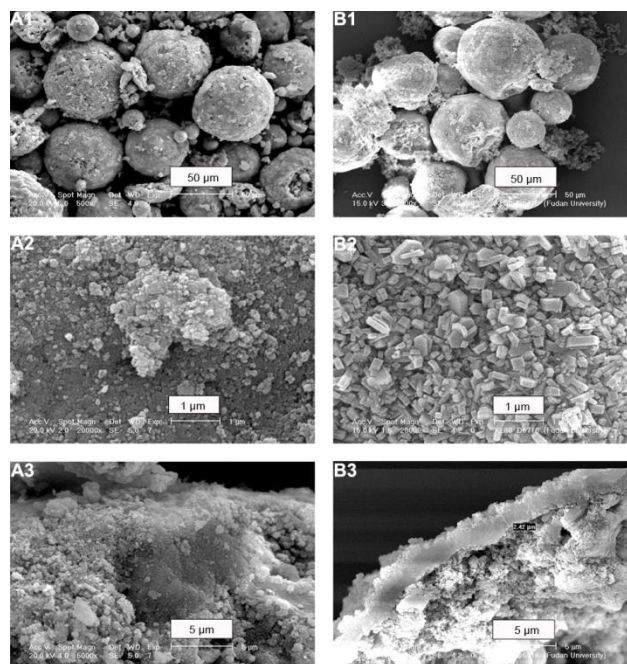


**Figure 1.** SEM images of FTC (A1) and FTC@S1 (B1) catalysts, external surface of FTC (A2) and FTC@S1 (B2), and cross section of FTC (A3) and FTC@S1 (B3).

$\text{N}_2$ -sorption (Figure 2-B) and acid-extraction (Table 1) experiments are adopted to prove the well coverage of zeolite shell on FTC core catalyst. In Figure 2-B, the FTC catalyst exhibits an obvious hysteresis loop at high relative pressure ( $P/P_0 = 0.75\text{-}0.9$ ) and a very low adsorption at low  $P/P_0$ , indicating mesoporosity of the sample. Its specific surface area and micropore surface area are  $45 \text{ m}^2\cdot\text{g}^{-1}$  (Brunauer-Emmett-Teller (BET) method) and  $5 \text{ m}^2\cdot\text{g}^{-1}$  (t-plot method), respectively. After coated by a zeolite shell without removal of SDA (i.e., the micropores in the zeolite shell are still filled by SDA), the hysteresis loop at high  $P/P_0$  value is significantly reduced, and the surface area is reduced to  $10 \text{ m}^2/\text{g}$  with negligible micropore surface area (Figure 2-B), which means that pores in the FTC core are blocked by a zeolite shell. However, after removing SDA in micropores by calcination, the hysteresis loop at high  $P/P_0$  is almost recovered, because guest  $\text{N}_2$  molecules can, once again, reach mesopores in the core via the SDA-removed zeolite shell. Additionally, due to the existence of micropore in zeolite shell, the uptake amount of  $\text{N}_2$  at low  $P/P_0$  value significantly increases. BET and micropore surface areas increase up to  $145$  and  $83 \text{ m}^2\cdot\text{g}^{-1}$ , respectively.

Results of the acid-extraction experiment further prove the intactness of zeolite shell. FTC and uncalcined FTC@S1 with SDA in its micropore are used. As shown in Table 1, almost all of Fe and Mn components in FTC sample are lost by acid erosion, while the uncalcined FTC@S1, in which micropores are still blocked by SDA, only loses 18% of Fe and 20% of Mn species due to protection of the micropore-blocked zeolite shell around. These results indicate that most of FTC cores have been completely covered by the zeolite shell in FTC@S1.

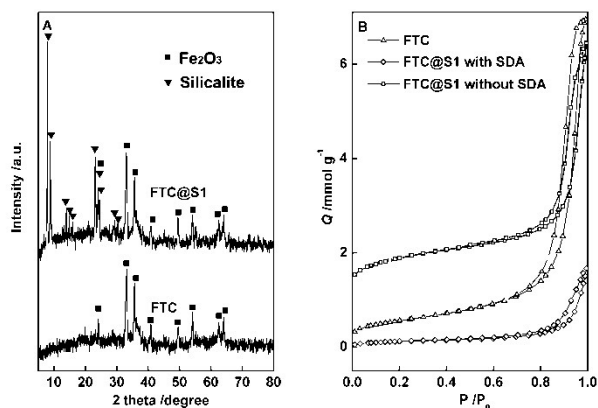


Figure 2. XRD patterns (A) and N<sub>2</sub> sorption isotherms (B).

Table 1. Element analysis of the samples by acid-extraction treatment

Catalyst	Fe content		Mn content		Fe lost	Mn lost
	/mg·g <sup>-1</sup>	/mg·g <sup>-1</sup>	/mg·g <sup>-1</sup>	/mg·g <sup>-1</sup>		
	before	after	before	after	/%	/%
FTC	303	<1	281	<1	>99	>99
FTC@S1	256	209	235	188	18	20

### 3.2 Catalytic performance

FTS tests are carried out for both parent FTC and FTC@S1 catalysts. All catalysts are loaded at the same amount of active components to ensure compatibility of the catalytic results, and each reaction result is obtained from a new run by reloading catalyst. The results of time of stream (TOS) present an induction period of less than 18 hours and good mass balance between inlet and effluent stream (Figure 3). Therefore, all catalytic data below are obtained at TOS of 24 hours within the steady period. Table 2 and Figures 4 and 5 show the experiment results at different temperatures. Both FTC and FTC@S1 present increasing CO conversion and CO<sub>2</sub> yield with elevating temperature, but the value of FTC@S1 is lower (Figure 4-A). If we define the ratios as CO conversion and light hydrocarbon (C<sub>1-4</sub>) selectivity on FTC divided by those on FTC@S1, it is very interesting that the ratio of CO conversion has a maximum at 603 K while the ratio of C<sub>1-4</sub> selectivity shows a minimum at the same temperature (Figure 4-B). Moreover, the ratios in the ends are close to 1 at both low (553 K) and high (653 K) temperatures. These interesting trends indicate that, with increasing temperature, difference of the FTS behaviors between FTC and FTC@S1 gradually enlarges in the range of low temperature but diminishes in the high temperature range.

As shown in Figure 5-A, the C<sub>2-4</sub><sup>=</sup>/C<sub>2-4</sub><sup>0</sup> ratio on FTC fades monotonously from 2.52 to 1.07 as reaction temperature ascends but the selectivity of C<sub>2-4</sub><sup>=</sup> changes a little. The latter could be explained by a compensating effect of the increase of C<sub>2-4</sub> selectivity and the decrease of C<sub>2-4</sub><sup>=</sup>/C<sub>2-4</sub><sup>0</sup> ratio. For the core-shell structured FTC@S1 (Figure 5-B), its C<sub>2-4</sub><sup>=</sup>/C<sub>2-4</sub><sup>0</sup> ratio presents similar trend to FTC at low temperature (< 603 K), but its value is much lower than that of FTC catalyst (Figure 5-A). However, when the temperature is over 603 K, C<sub>2-4</sub><sup>=</sup>/C<sub>2-4</sub><sup>0</sup> of

FTC@S1 dramatically increases, leading to a significant rise of C<sub>2-4</sub><sup>=</sup> selectivity despite of slight decline of total C<sub>2-4</sub> selectivity. At 653 K, both C<sub>2-4</sub><sup>=</sup>/C<sub>2-4</sub><sup>0</sup> ratio (1.85) and selectivity of C<sub>2-4</sub><sup>=</sup> (24.8%) of FTC@S1 are higher than those of FTC (C<sub>2-4</sub><sup>=</sup>/C<sub>2-4</sub><sup>0</sup> ratio = 1.07 and C<sub>2-4</sub><sup>=</sup> selectivity = 20.4%).

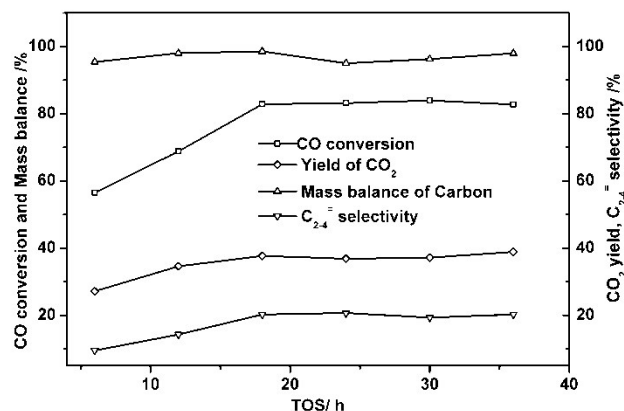


Figure 3. Performance of FTC on TOS. Reaction: T=653K, P=1.0MPa.

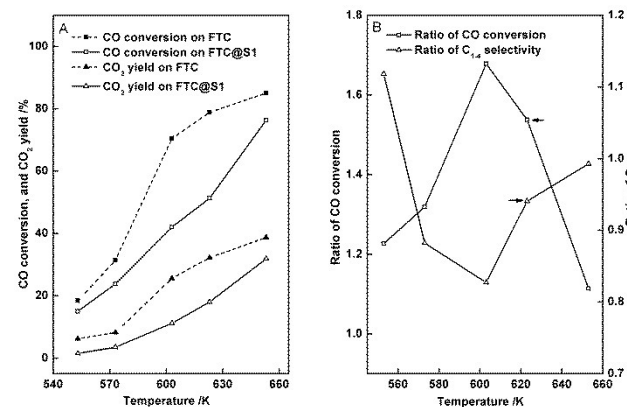


Figure 4. CO conversion and CO<sub>2</sub> yield (A), and ratios of CO conversion and C<sub>1-4</sub> selectivity (B).

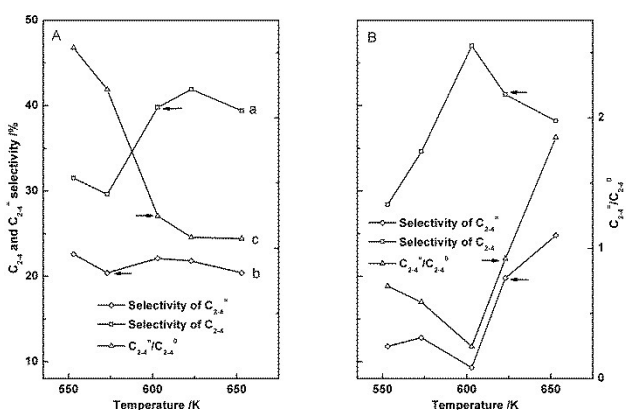


Figure 5. Selectivity of C<sub>2-4</sub> hydrocarbons, selectivity of C<sub>2-4</sub><sup>=</sup>, and the C<sub>2-4</sub><sup>=</sup>/C<sub>2-4</sub><sup>0</sup> ratio on FTC (A) and FTC@S1 (B).

**Table 2.** Effects of reaction temperature on FTC and FTC@S1 catalysts

Catalysts	FTC					FTC@S1				
Temperature /K	553	573	603	623	653	553	573	603	623	653
H <sub>2</sub> /CO ratio /v/v	1.5	1.5	1.5	1.5	1.5	1.5	1.5	1.5	1.5	1.5
Pressure /MPa	1.0	1.0	1.0	1.0	1.0	1.0	1.0	1.0	1.0	1.0
WHSV <sup>a</sup> /g•h <sup>-1</sup> •(g Fe) <sup>-1</sup>	3.9	3.9	3.9 (6.6) <sup>c</sup>	3.9	3.9	3.9	3.9	3.9	3.9	3.9
CO conversion /C-mol%	18.4	31.4	70.5 (49.9)	78.9	85.0	15.0	23.8	42.0	51.3	76.3
CO <sub>2</sub> yield /C-mol%	6.2	8.2	25.6 (19.6)	32.2	38.7	1.5	3.5	11.2	18.0	31.9
Mass balance /C-mol%	99.8	94.2	95.3 (98.8)	95.9	97.5	99.0	97.7	96.4	97.1	97.7
Selectivity <sup>b</sup> /C-mol%										
CH <sub>4</sub>	13.0	13.1	21.0 (23.8)	26.2	29.5	11.4	13.8	26.5	31.1	31.2
C <sub>2</sub> H <sub>4</sub>	4.4	3.2	2.3 (3.5)	2.2	2.3	0.8	0.9	0.7	2.6	5.0
C <sub>2</sub> H <sub>6</sub>	4.5	4.7	9.4 (10.7)	11.2	11.2	6.6	8.7	15.9	12.9	9.0
C <sub>3</sub> H <sub>6</sub>	10.2	9.5	11.2 (12.3)	11.4	10.8	5.3	5.7	3.9	9.8	11.3
C <sub>3</sub> H <sub>8</sub>	2.2	2.3	5.0 (4.7)	5.7	5.2	6.2	8.4	14.8	6.4	3.1
C <sub>4</sub> H <sub>8</sub>	8.0	7.7	8.6 (11.3)	8.2	7.3	5.7	6.2	4.7	7.4	8.5
C <sub>4</sub> H <sub>10</sub>	2.2	2.2	3.3 (2.8)	3.2	2.6	3.8	4.7	7.0	2.2	1.3
C <sub>5</sub> <sup>+</sup>	55.5	57.3	39.2 (30.9)	31.9	31.1	60.2	51.6	26.5	27.6	30.6
C <sub>1-4</sub>	44.5	42.7	60.8 (69.1)	68.1	68.9	39.8	48.4	73.5	72.4	69.4
C <sub>2-4</sub> <sup>=</sup>	22.6	20.4	22.1 (27.2)	21.8	20.4	11.8	12.8	9.3	19.8	24.8
C <sub>2-4</sub> <sup>=</sup> /C <sub>2-4</sub> <sup>0</sup>	2.54	2.22	1.25 (1.49)	1.08	1.07	0.71	0.59	0.25	0.92	1.85
C <sub>2-4</sub> <sup>=</sup> /C <sub>2-4</sub>	0.72	0.69	0.56 (0.60)	0.52	0.52	0.42	0.37	0.20	0.48	0.65
1-C <sub>4</sub> <sup>=</sup> /C <sub>4</sub> <sup>=</sup>	0.57	0.53	0.26 (0.47)	0.22	0.23	0.17	0.17	0.17	0.18	0.17

<sup>a</sup>Value of WHSV is calculated as the weight of CO per hour divided by the weight of Fe component.

<sup>b</sup>Selectivities are calculated as product distribution in hydrocarbon products.

<sup>c</sup>Data in parentheses are obtained at 6.6 g•h<sup>-1</sup>•(g Fe)<sup>-1</sup> to make the conversion of FTC close to that of FTC@S1.

It is noted that conversions of FTC and FTC@S1 are close to each other at both high and low temperatures (553 and 673 K, Figure 4), but their values are very different between, especially those at 603 K. To more rationally compare selectivities between these two catalysts, we also adjust the WHSV to 6.6 g•h<sup>-1</sup>•(g Fe)<sup>-1</sup> to reduce conversion of FTC at 603 K to close to that of FTC@S1 (see the data in parentheses of Table 2). With lower conversion, C<sub>2-4</sub><sup>=</sup> selectivity and C<sub>2-4</sub><sup>=</sup>/C<sub>2-4</sub><sup>0</sup> ratio of FTC increase to 27.2% and 1.49 from 22.1% and 1.25, respectively. As result, the gap of selectivities between FTC and FTC@S1 at similar conversion even augments comparing to the results under the same WHSV value, further proving the effect of silicalite-1 shell in FTS reaction.

FTC@S1 also shows quite different behavior on 1-butylene/butylenes ratio (1-C<sub>4</sub><sup>=</sup>/C<sub>4</sub><sup>=</sup>) from that of FTC core catalyst (Table 2). 1-C<sub>4</sub><sup>=</sup>/C<sub>4</sub><sup>=</sup> ratio on FTC decreases with temperature from 553 to 603 K and then keeps constant at a value of about 0.2. However, for FTC@S1, the ratio is as low as 0.17, which keeps steady within the whole range of reaction temperature, indicating that isomerization of 1-butylene is much easier on FTC@S1 than that on FTC.

## 4. Discussion

### 4.1 Role of the zeolite shell

From the above work, it can be seen that the product distribution of FTC@S1 and FTC is very different because of the existence of zeolite shell. As reported in the previous literatures, the selectivity of olefin products is affected by pellet size of catalysts and bed residence time.<sup>17</sup> The former would mainly influence diffusion of CO and olefin products within pellets and thereby impact the intra-pellet secondary reactions. The latter would enhance the hydrogenation/chain growth reactions in the catalyst bed, i.e., inter-pellet secondary reactions. Therefore, besides the nature of the catalyst itself, the selectivity of olefin products can be also affected by diffusion of reactants and products as well as the bed residence time. The existence of the microporous silicalite-1 shell may affect diffusions of various reactants and products and thereby change the olefin yield. The previous literature has suggested that FTS catalyst coated with silicalite-1 could result in a higher H<sub>2</sub>/CO ratio within the shell for the resistance on CO diffusion and reduce secondary reactions of C<sub>2-4</sub><sup>=</sup>,<sup>42</sup> which thereby improves the selectivity of light hydrocarbons and C<sub>2-4</sub><sup>=</sup>. Remarkably, as observed in our results

(see Section 3.2), the silicalite-1 shell has a much more complex role in FTS, which leads to a very special temperature-dependent effect on  $C_{2-4}^-$  selectivity. Herein we propose a scheme as shown in Figure 6 and then analyze the special reaction behaviors of core-shell catalyst by comparing them with those of naked FTC.

As shown in Figure 6, three main steps are included in FTS reaction process: (1) Reactants ( $CO$  and  $H_2$ ) diffuse into ( $d_1$  and  $d_2$ , respectively) and are adsorbed on the surface of catalyst pellets. (2) The primary  $C_{2-4}^-$  products are generated via FTS, which may take part in the secondary hydrogenation reactions to  $C_{2-4}^0$  ( $r_h$ ) or chain growth to long chain hydrocarbons ( $r_c$ ) during its diffusing process ( $d_3$ ) in the same pellet (the intra-pellet secondary reaction). (3)  $C_{2-4}^-$  products, escaping into the gas flow, would be re-adsorbed in the pellets in the downstream of catalyst bed ( $d_4$ ) and participate in the secondary reactions (inter-pellet secondary reactions). On the basis of this scheme, the effects of the zeolite shell on these three steps could be discussed combined with the experimental results.

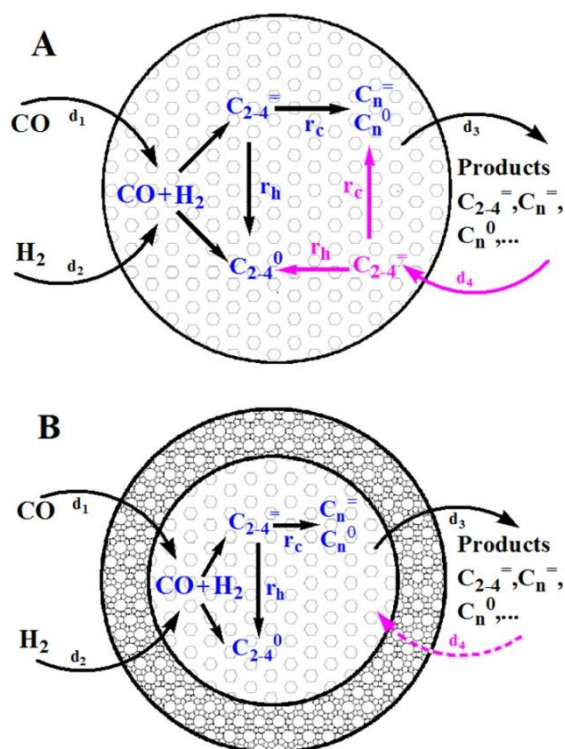


**Figure 6.** Scheme of light olefin formation in FTS on FTC and FTC@S1 catalysts.

**4.1.1 Diffusion limitation on reactants.** Diffusion restriction of catalyst pellets may promote the  $H_2/CO$  ratio within the pellet somewhat higher than that in the fed flow since the diffusion rate of  $CO$  ( $d_1$ ) is slower than that of  $H_2$  ( $d_2$ ).<sup>42</sup> It was proposed that the intra-pellet diffusion effect is related to a structure parameter of catalyst pellets ( $\chi$ ):  $\chi = L^2 \cdot \theta / R_p$ , here  $L$  is the pellet size,  $R_p$  is the pore size of catalyst pellets and  $\theta$  is the density of active sites.<sup>13, 27</sup> The parameter  $\theta$  is with respect to the reaction rate, and  $L$  and  $R_p$  are related to the diffusion rate. Therefore, the extent of diffusion limitation on  $CO$  is

proportional to the ratio of consumption rate ( $\theta$ )/diffusion rate ( $R_p/L^2$ ) of  $CO$ .

At low temperature (553 K), the influence of diffusion limitation is low because  $CO$  consumption is so slow that  $CO$  conversion and product distribution on FTC and FTC@S1 are similar. The  $CO$  consumption rate rapidly increases with reaction temperature, which enhances the effect of diffusion limitation. However, as the temperature is higher than 603 K, due to the heavier stretching vibration of both zeolite framework and guest molecules, the increment of  $CO$  diffusion rate ( $R_p/L^2$ ) is probably larger than that of  $CO$  consumption rate ( $\theta$ ), leading to the decrease of  $\chi$ . The effect of diffusion limitation of zeolite shell gradually fades with increasing temperature and the two catalysts show similar activity and product distribution again at 653 K. The severest effect of diffusion limitation at 603 K results in relatively lower  $CO$  conversion and higher intra-pellet  $H_2/CO$  ratio on FTC@S1 than those on FTC, both of which would lead to the minimum of the ratio of  $C_{1-4}$  selectivity on FTC to that on FTC@S1 at 603 K (Figure 4-B and Table 2).

**4.1.2 Intra-pellet secondary reaction.** The previous literature suggested that  $C_{2-4}^-$  products could diffuse out of the zeolite shell freely so that secondary reactions of  $C_{2-4}^-$  within catalyst pellets are not obvious.<sup>42</sup> Other researchers indicated that water produced in FTS would be confined in Co-based catalyst pellet with a silica shell and inhibit secondary reactions of  $C_{2-4}^-$  in the pellet.<sup>43</sup> However, our results exhibit different trends in the low temperature range (553-603 K). More significant secondary reactions of  $C_{2-4}^-$  happen on FTC@S1 at low temperature, leading to lower  $C_{2-4}^-$  selectivity and  $C_{2-4}^-/C_{2-4}^0$  ratio on FTC@S1 (Figure 5). This could be attributed to relatively longer retention time of the primary  $C_{2-4}^-$  products and higher  $H_2/CO$  within the shell. These results clearly show that silicalite-1 shell would cause diffusion restriction on  $C_{2-4}^-$  within catalyst pellets, leading to enhanced intra-pellet secondary reactions of  $C_{2-4}^-$ .

**4.1.3 Inter-pellet secondary reaction.** When the temperature elevates to the high temperature range (above 603 K), the diffusion limitation on  $CO$  of zeolite shell gradually decreases due to the more vigorous stretching vibration of zeolite framework and guest molecules. For the same reason, the diffusion restriction on  $C_{2-4}^-$  would be also reduced and  $C_{2-4}^-$  tend to escape out of catalyst pellets before being converted. However, because of the possible inter-pellet secondary reaction via re-adsorption in the downstream of catalyst bed,  $C_{2-4}^-/C_{2-4}^0$  ratio of FTC decreases continuously (Figure 5-A). Conversely, as illustrated in Figure 6, this process ( $d_4$ ) is reduced on the FTC@S1 pellets because of the existence of zeolite shell that partially blocks the mesoporous entrances of core particle and decreases the effective area for guest molecule diffusion (also see the controlled test of ethylene hydrogenation in the next section) so that  $C_{2-4}^-/C_{2-4}^0$  ratio on this catalyst exhibits a trend inverting to that of FTC, i.e., it increases with reaction temperature. The datum even reaches 1.7 times than that of FTC at 653 K (Figure 5-B). Because of the above reasons, the sample with zeolite shell achieves a

synchronous increase of CO conversion and  $C_{2-4}^{\pm}$  selectivity which is very important information for design of FTS catalysts for  $C_{2-4}^{\pm}$ .

#### 4.2 Verification of effects of zeolite shell on secondary reactions

As discussed above, the existence of silicalite-1 shell results in diffusion resistance on CO and olefin products at low temperature, which would lead to a higher intra-pellet  $H_2/CO$  ratio and enhanced intra-pellet secondary reactions. At the same time, the silicalite-1 shell can also prohibit the inter-pellet secondary reaction, especially at high temperature. To prove the roles of silicalite-1 shell, three controlled reactions were conducted: (1) effects of  $H_2/CO$  ratio on the activity and selectivity of FTC catalyst to simulate the diffusion limitation of silicalite-1 shell on reactants; (2) effects of WHSVs on the product distribution of FTC catalyst to verify that the longer bed residence time would lead to more serious secondary reactions under our conditions; and (3) hydrogenation of ethylene on both FTC and FTC@S1 catalysts to prove the effect of zeolite shell on hindrance of the inter-pellet secondary reaction.

**4.2.1 Effect of  $H_2/CO$  ratio on activity and selectivity of FTC catalyst.** As shown in Figure 7, with  $H_2/CO$  ratio rising,  $C_{2-4}^{\pm}$  and  $C_{1-4}$  selectivity increases whereas  $C_{2-4}^{\pm}/C_{2-4}^0$  ratio drops. The selectivity of  $C_{2-4}^{\pm}$  increases before  $H_2/CO$  of 5/5 and then drops dramatically. Considering the high  $H_2/CO$  (6/4, dash line in Figure 7) in our FTS reactions and that the existence of zeolite shell would further increase this ratio due to the diffusion restriction on CO, these results are consistent with the performance of FTC@S1 in the low temperature range where the effect of diffusion limitation is significant (Figures 4-B and 5-B, and Sections 4.1.1 and 4.1.2). It implies that the higher intra-pellet  $H_2/CO$  ratio can cause higher  $C_{1-4}$  selectivity, higher  $C_{2-4}^{\pm}$  selectivity, lower  $C_{2-4}^{\pm}$  selectivity and  $C_{2-4}^{\pm}/C_{2-4}^0$  ratio due to higher diffusion limitation of the silicalite-1 shell on CO. However, at high temperature, light olefin selectivity is mainly determined by the inter-pellet secondary reaction and therefore it presents a reversed tendency as described in Section 4.1.3.

#### 4.2.2 Effect of WHSVs on product distribution of FTC catalyst.

It is clearly shown in Figure 8 that the residence time of reaction gas on catalyst bed greatly influences occurrence of secondary reactions. The selectivity of  $C_{2-4}^{\pm}$  increases whereas that of the corresponding paraffins ( $C_{2-4}^0$ ) decreases with increase of space velocity (Figure 8-A), leading to the great increase of  $C_{2-4}^{\pm}/C_{2-4}^0$  ratio (Figure 8-B). This indicates that considerable inter-pellet secondary hydrogenation of  $C_{2-4}^{\pm}$  happens on FTC. Additionally,  $1-C_4^{\pm}/C_4^{\pm}$  ratio enhances with increasing space velocity (Figure 8-B), indicating that 1-butylene is the primary product and its isomer is the secondary one. Therefore, hydrogenation and isomerization are the main secondary reactions of  $C_{2-4}^{\pm}$  here, which is consistent with the results of FTS reaction in our experiments shown above (Section 3.2).

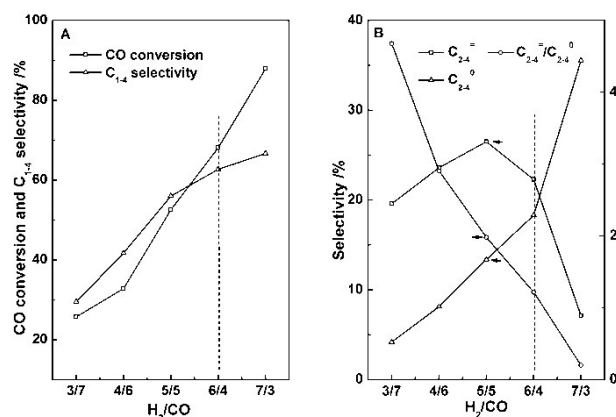


**Figure 7.** Effect of the  $H_2/CO$  ratio on CO conversion and  $C_{1-4}$  selectivity. Reaction condition:  $T = 603$  K,  $P = 1.0$  MPa. The dash line represents the value of  $H_2/CO$  ratio in our FTS tests.

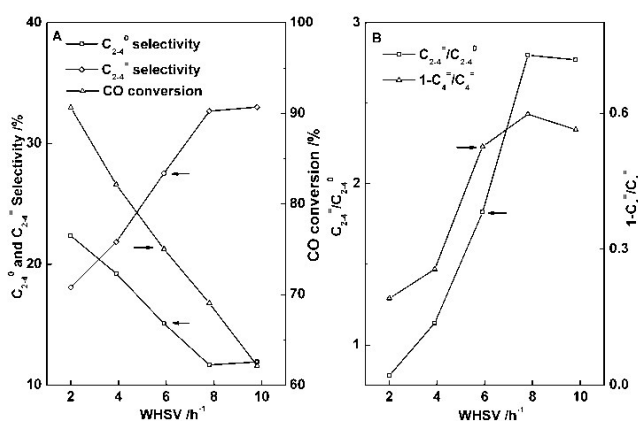


**Figure 8.** Effect of WHSV on FTC on  $C_{2-4}^{\pm}$  and  $C_{2-4}^0$  selectivity (A),  $C_{2-4}^{\pm}/C_{2-4}^0$  and 1-butylene/butylenes ratios (B), and CO conversion and selectivity of  $CH_4$  and  $C_5^+$  (C). Reaction condition:  $H_2/CO = 3/2$ ,  $T = 623$  K,  $P = 1.0$  MPa.

#### 4.2.3 Simulation of secondary reactions of olefin by ethylene hydrogenation.

To further prove that the zeolite shell can suppress inter-pellet secondary reaction of  $C_{2-4}^{\pm}$  as discussed above, a controlled experiment of ethylene hydrogenation was carried out by switching to a mixing gas of ethylene and hydrogen after 24 hours of reaction of syngas to ensure the active components in the same state as that in FTS reaction. The TOS experiment result (Figure 3) indicates that the selected time for pre-reaction of FTS is suitable due to its steady reaction periods. Concentrations of  $CH_4$  and  $C_3^+$  hydrocarbons in the effluent gas are rather low (Table 3), also implying that hydrogenolysis and secondary chain growth reactions are not obvious in our catalytic system. Table 3 clearly shows that a considerable amount of ethylene is hydrogenated on FTC. The ethane/ethylene ( $C_2^0/C_2^{\pm}$ ) ratio increases with increasing reaction temperature. At 653 K, 1.0 MPa and hydrogen/ethylene ( $H_2/C_2^{\pm}$ ) of 2:1, about 44 % of ethylene is hydrogenated to ethane and the  $C_2^0/C_2^{\pm}$  ratio gets to 0.81. This is consistent with our results of FTS, in which  $C_2$

$\text{C}_2^=/\text{C}_{2-4}^0$  ratio decreases with increasing reaction temperature on FTC (Figure 5-A). On FTC@S1, although  $\text{C}_2^0/\text{C}_2^=$  ratio also increases with temperature, its values are obviously lower than those on FTC even under the conditions of a much higher  $\text{H}_2/\text{C}_2^=$  ratio (3:1) and a higher pressure (2.5 MPa), which demonstrates the suppression of ethylene hydrogenation on the core-shell catalyst. The zeolite shell may either blocks the active sites on the external surface of FTC catalyst or reduces the flux of reactants into the core catalyst particles due to decrease of effective diffusion area.<sup>45,46</sup> Such role of zeolite shell can successfully retard olefins to contact to the active species on catalyst pellets for hydrogenation of ethylene (Table 3) and also for inter-pellet secondary reactions (Figure 6, d4), and thereby ensures the increment of  $\text{C}_{2-4}^=/\text{C}_{2-4}^0$  ratio as well as  $\text{C}_{2-4}^=$  selectivity of FTS process in the high temperature range (Figure 5-B).

**Table 3.** Results of ethylene hydrogenation on FTC and FTC@S1 catalysts

Catalyst	FTC			FTC@S1			
Temperature /K	553	623	653	553	623	653	653
H <sub>2</sub> flow rate /ml·min <sup>-1</sup>	60	60	60	90	90	90	60
C <sub>2</sub> H <sub>4</sub> flow rate /ml·min <sup>-1</sup>	30	30	30	30	30	30	30
Pressure /MPa	1.0	1.0	1.0	2.5	2.5	2.5	1.0
WHSV <sup>a</sup> /g·h <sup>-1</sup> ·(g Fe) <sup>-1</sup>	3.9	3.9	3.9	3.9	3.9	3.9	3.9
C <sub>2</sub> H <sub>4</sub> conversion /%	10.3	27.5	45.1	2.5	3.6	12.7	0.7
Effluent composition /%							
CH <sub>4</sub>	0.2	0.2	0.3	<0.1	0.1	0.5	<0.1
C <sub>2</sub> H <sub>4</sub>	89.7	72.5	54.9	97.5	96.4	87.3	99.3
C <sub>2</sub> H <sub>6</sub>	9.9	27.1	44.5	12.4	3.24	10.9	0.6
C <sub>3</sub>	0.1	0.1	0.1	<0.1	0.1	0.6	<0.1
C <sub>4</sub>	0.2	0.1	0.2	0.1	0.2	0.6	<0.1
$\text{C}_2^0/\text{C}_2^=$	0.11	0.37	0.81	0.02	0.03	0.13	<0.01

## 5. Conclusion

In this work, the effects of silicalite-1 shell on core-shell catalyst for producing  $\text{C}_{2-4}^=$  are systematically analyzed. The core-shell catalyst is synthesized by directly hydrothermal treating a seeded industrial Fe-Mn-Cu/SiO<sub>2</sub> catalyst. The zeolite shell is found to have different effects on diffusion of reactants and products with various molecule sizes at different temperatures. An interesting temperature-dependent effect of the zeolite shell is declared for the first time by comparing the catalytic performance of catalysts with and without a zeolite shell. Remarkably, a reverted change of  $\text{C}_{2-4}^=/\text{C}_{2-4}^0$  ratio and a corresponding increase of  $\text{C}_{2-4}^=$  selectivity are discovered on the core-shell catalyst in the high reaction temperature range, which could be rationally attributed to the limitation of zeolite shell on the inter-pellet secondary hydrogenation of  $\text{C}_{2-4}^=$ . Synchronous increase of CO conversion and  $\text{C}_{2-4}^=$  selectivity can be achieved. This observation opens a new view for the design of FTS catalysts for  $\text{C}_{2-4}^=$  and other catalysts for complex reaction networks.

## Acknowledgements

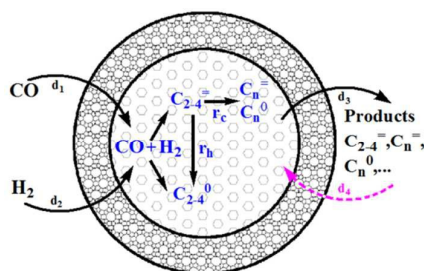
This work is supported by National Key Basic Research Program of China (2013CB934101), NSFC (21433002, 21403303 and 21573046), Science and Technology Commission of Shanghai Municipality (11JC1400400), National Plan for Science and Technology of Saudi Arabia (14-PET827-02), Sinopec (X514005) and Royal Academy of Engineering-Newton Funds of UK.

## Notes and references

- D. Chen, K. Moljord, T. Fuglerud and A. Holmen, *Microporous and Mesoporous Mater.*, 1999, **29**, 191-203.
- J. Q. Chen, A. Bozzano, B. Glover, T. Fuglerud and S. Kvisle, *Catal. Today*, 2005, **106**, 103-107.
- P. Wang, A. Lv, J. Hu, J. a. Xu and G. Lu, *Ind. Eng. Chem. Res.*, 2011, **50**, 9989-9997.
- X. Dupain, R. A. Krul, C. J. Schaverien, M. Makkee and J. A. Moulijn, *Appl. Catal. B: Environmental*, 2006, **63**, 277-295.
- T. V. Malleswara Rao, X. Dupain and M. Makkee, *Microporous and Mesoporous Mater.*, 2012, **164**, 148-163.
- M. Janardanao, *Ind. Eng. Chem. Res.*, 1990, **29**, 1753-1771.
- H. M. T. Galvis, J. H. Bitter, C. B. Khare, M. Ruitenbeek, A. I. Dugulan and K. P. d. Jong, *SCIENCE*, 2012, **335**, 4.
- D. Wang, X. Zhou, J. Ji, X. Duan, G. Qian, X. Zhou, D. Chen and W. Yuan, *J. Mater. Chem. A*, 2015, **3**, 4560-4567.
- M. E. Dry and A. P. Steynberg, in *Stud. Surf. Sci. Catal.*, eds. A. R. Steynberg and M. E. Dry, Elsevier, Amsterdam, 2004, vol. 152, ch. 5, pp. 406-481.
- H. Schulz and M. Claeys, *Appl. Catal., A*, 1999, **186**, 71-90.
- V. Sage and N. Burke, *Catal. Today*, 2011, **178**, 137-141.
- M. L. Turner, N. Marsih, B. E. Mann, R. Quyoun, H. C. Long and P. M. Maitlis, *J. Am. Chem. Soc.*, 2002, **124**, 10456-10462.
- E. Iglesia, S. C. Reyes and R. J. Madon, *J. Catal.*, 1991, **129**, 238-256.
- F. Fiore, L. Lietti, G. Pederzani, E. Tronconi, R. Zennaro and P. Forzatti, in *Stud. Surf. Sci. Catal.*, eds. X. Bao and Y. Xu, Elsevier Science B.V., Amsterdam, 2004, vol. 147, ch4, pp. 289-294.
- B. Shi and B. H. Davis, *Appl. Catal., A*, 2004, **277**, 61-69.
- E. Iglesia, *Appl. Catal., A*, 1997, **161**, 59-78.
- E. Iglesia, S. C. Reyes, R. J. Madon and S. L. Soled, *Adv. Catal.*, 1993, **39**, 221-302.
- J. M. Bucher and J. W. Schwank, *Fuel Process. Technol.*, 2009, **90**, 1009-1015.
- X. Liu, A. Hamasaki, T. Honma and M. Tokunaga, *Catal. Today*, 2011, **175**, 494-503.
- E. Rytter, S. Eri, T. H. Skagseth, D. Schanke, E. Bergene, R. Myrstad and A. Lindvåg, *Ind. Eng. Chem. Res.*, 2007, **46**, 9032-9036.
- E. Iglesia, S. I. Soled and R. A. Fiato, *J. Catal.*, 1992, **137**, 212-224.
- F. G. Botes and N. S. Govender, *Energy Fuels*, 2007, **21**, 3095-3101.
- S. Sharifnia, Y. Mortazavi and A. Khodadadi, *Fuel Process. Technol.*, 2005, **86**, 1253-1264.
- F. Kapteijn, R. M. d. Deugd and J. A. Moulijn, *Catal. Today*, 2005, **105**, 350-356.
- R. M. d. Deugd, F. Kapteijn and J. A. Moulijn, *Catal. Today*, 2003, **79-80**, 495-501.

26. H. A. J. v. Dijk, J. H. B. J. Hoebink and J. C. Schouten, *Chem. Eng. Sci.*, 2001, **56**, 1211-1249.
27. R. J. Madon and E. Iglesia, *J. Catal.*, 1993, **139**, 576-590.
28. R. J. Madon, S. C. Reyes and E. Iglesia, *J. Phys. Chem.*, 1991, **95**, 7795-7804.
29. A. N. Pour and M. R. Housaindokht, *J. Nat. Gas Sci. Eng.*, 2013, **14**, 204-210.
30. S. Soled, E. Iglesia and R. A. Fiato, *Catal. Lett.*, 1990, **7**, 271-280.
31. L. Chen, W. Song, Y. Zhang, W. Yang, L. Wu and Y. Tang, *Chin. J. Catal.*, 2014, **35**, 1661-1668.
32. D. B. Bukur, X. Lang, A. Akgerman and Z. Feng, *Ind. Eng. Chem. Res.*, 1997, **36**, 2580-2587.
33. D. S. Jordan and A. T. Bell, *J. Catal.*, 1987, **107**, 338-350.
34. D. S. Jordan and A. T. Bell, *J. Phys. Chem.*, 1986, **90**, 4797-4805.
35. R. Snel, *J. Mol. Catal.*, 1989, **54**, 103-117.
36. R. Snel, *J. Mol. Catal.*, 1989, **54**, 119-130.
37. R. Snel and R. L. Espinoza, *J. Mol. Catal.*, 1987, **43**, 237-347.
38. D. S. Jordan and A. T. Bell, *J. Catal.*, 1987, **107**, 338-350.
39. R. M. M. Abbaslou, J. S. S. Mohammadzadeh and A. K. Dalai, *Fuel Process. Technol.*, 2009, **90**, 849-856.
40. N. Tsubaki and K. Fujimoto, *Fuel Process. Technol.*, 2000, **62**, 173-186.
41. G. Junhu, W. Baoshan, Z. Liping, Y. Yong, H. Xu, X. Yuanyuan and L. Yongwang, *Chin. J. Catal.*, 2011, **32**, 1790-1802.
42. N. Jiang, G. Yang, X. Zhang, L. Wang, C. Shi and N. Tsubaki, *Catal. Commun.*, 2011, **12**, 951-954.
43. B. Zeng, B. Hou, L. Jia, D. Li and Y. Sun, *J. Mol. Catal. A: Chem.*, 2013, **379**, 263-268.
44. X. D. Wang, W. L. Yang, Y. Tang, Y. J. Wang, S. K. Fu and Z. Gao, *Chem. Commun.*, 2000, 2161-2162.
45. A. J. Burggraaf, *J. Membr. Sci.*, 1999, **155**, 45-65.
46. S. Karoor and K. Sirkar, *Ind. Eng. Chem. Res.*, 1993, **32**, 674-684.

## Table of Content

**Fe-Mn-Cu/SiO<sub>2</sub>@Silicalite-1 Catalyst for CO Hydrogenation: Role of Zeolite Shell on Light-Olefin Production**

Weilin Song, Bin Zhang, Lifeng Chen, Jing Shi, Xiaowei Cheng, Lianghua Wu, Weimin Yang, Yahong Zhang, Yewu Tao, Yi Tang\*

The silicalite-1 coated catalyst presents a unique temperature-depended performance due to the zeolite shell's diffusion limitation on reactants and products and suppression of secondary reactions on downstream catalysts.